May, 2016

A Wearable Conductivity Sensor for Wireless Real-time Sweat Monitoring

Gengchen Liu
Che-Ting Ho
Nate Slappey
Zhixuan Zhou
Samuel Snelgrove, et al.

Sensors and Actuators B 227 (2016) 35–42

Contents lists available at ScienceDirect

Sensors and Actuators B: Chemical

journal homepage: www.elsevier.com/locate/snb

A wearable conductivity sensor for wireless real-time sweat monitoring

G. Liu[a], C. Ho[b], N. Slappey[b], Z. Zhou[b], S.E. Snelgrove[c], M. Brown[b], A. Grabinski[b], X. Guo[d], Y. Chen[b], K. Miller[e], J. Edwards[c], T. Kaya[b,*]

[a] Department of Electrical and Computer Engineering, University of California at Davis, Davis 95616, USA
[b] School of Engineering and Technology, Central Michigan University, Mt. Pleasant 48859, USA
[c] School of Health Sciences, Central Michigan University, Mt. Pleasant 48859, USA
[d] Department of Electrical and Computer Engineering, University of California at San Diego, La Jolla 92093, USA
[e] School of Rehabilitation and Medical Sciences, Central Michigan University, Mt. Pleasant 48859, USA

ARTICLE INFO

Article history:
Received 7 October 2015
Received in revised form
10 December 2015
Accepted 11 December 2015
Available online 15 December 2015

Keywords:
Wearable device
Sweat sensing
Conductivity sensor
Physiological monitoring
Electrochemical Impedance Spectroscopy

ABSTRACT

We designed, fabricated, and tested a sweat-based conductivity sensor device toward a real-time, non-invasive physiological condition monitoring device for humans. Sweat collector, conductivity sensor, and the interfacing circuit were developed and combined to form a wearable device. Polydimethylsiloxane (PDMS) based sweat collector was fabricated to collect sweat from skin using the hydraulic pumping action of sweat glands. PDMS sweat collectors were prepared using 3D printed plastic molds. The interfacing circuit was designed based on the results of the conductivity sensor that was characterized by the Electrochemical Impedance Spectroscopy. Human testing was performed to prove the feasibility of the proposed sweat sensing system for the real-time non-invasive monitoring of human sweat. The first reading from the device was obtained in 7–20 min depending on the subject and the location of the electrodes. Sweat rate plateaued after a consistent work load of exercise, as was expected. The sweat conductivity decayed after the first readings due to the initial mineral content of the skin. Finally, an increasing trend in sweat conductivity was observed which may be due to subjects' changing hydration level.

1. Introduction

As one of the most readily accessible human biofluids, sweat can be used to provide information about one's electrolyte concentrations [1,2]. Hypohydration and hyperhydration have received the greatest attention but, as Maughan and Shireffs wrote, if the desired goal is to provide individualized hydration and rehydration prescriptions it is as important to monitor the plasma osmolality [3]. The American College of Sports Medicine Position Stand on Exercise and Fluid Replacement states that, "Because there is considerable variability in sweating rates and sweat electrolyte content between individuals customized fluid replacement programs are recommended." [4]. Sweat is hypotonic when compared to plasma but the actual composition varies as the result of many factors including sweat rate, acclimation and diet [3]. Currently, blood serum analysis is considered to be the gold standard method of electrolyte concentrations. However, this technique is highly invasive and is impractical for real-time, on-the-field assessment of hydration during competition [5,6]. Alternately, real-time sampling of sweat has become a possibility as a potential proxy measure for plasma, although further work is needed to establish validity.

Using sweat as a biomarker has recently drawn attention and several studies have been carried out to explore the potential of sweat sensing [2,7,8]. Approaches include, but are not limited to, optical detection with porous fabrics [7], attachable tattoo paper with Ion Selective Electrodes (ISEs) [9], and incorporating organic dyes [8]. Recently, Electrochemical Impedance Spectroscopy (EIS) has been successfully utilized for conductometric sensing applications [10–13]. Conductometric-based sensors offer simplicity and ease of manufacturability making the technique very popular in sensing devices such as biomedical diagnostic probes, sensors for environmental monitoring, and microfluidic biosensors [10,14,15].

Recent growth in wrist watch-based wearable devices, such as Fitbit®, G-watch, and heart-rate monitors [16–18], has led several researchers to focus on the development of a wearable device that can measure other physiologic processes during exercise [19,20].

* Corresponding author.
E-mail address: kaya2t@cmich.edu (T. Kaya).

http://dx.doi.org/10.1016/j.snb.2015.12.034
0925-4005/

Previous work includes monitoring of body temperature, heart rate, accidental falls, and movement [20–22]. The idea of using wearable devices for monitoring sweat electrolyte concentration is a fairly new but emergent concept, primarily targeting collegiate and professional athletes. De Rossi and his colleagues proposed a device that measures sweat rate by integrating two humidity sensors on a textile substrate whereby differential outputs were used to calculate the sweat rate [23]. Diamond's group fabricated an optical sweat-based pH sensor by incorporating a pH sensitive dye with a micro-LED/photodetector pair [7].

A wearable device for physiological activity monitoring can be broken down into three parts; data collection, data processing, and transmission [19]. Sweat monitoring, in particular, can be detailed into the following steps: (1) collecting sweat, (2) sensing the sweat analyte, (3) circuit interface, (4) data processing, and (5) transmission.

In this paper, we present a conductivity sensor based sweat sensing system packaged as a wrist watch. The prototype collects sweat from the forearm, reads the conductivity value and transmits the data wirelessly to a smart phone via a Bluetooth® transceiver. The results show that the proposed system has a potential ground-breaking ramification as it opens the gate for assessing real-time sweat electrolyte status of athletes during practice and competition.

2. Results and discussion

2.1. Sweat collector

The human body secretes sweat through eccrine sweat glands mainly to regulate the body temperature [24]. There have been many different methods used to measure the density and distribution of eccrine sweat gland distribution in humans. Scientists have used thermal, exercise, pharmacological, electrophysiological, and pharmacological stimuli to assess sweat. No matter the methodology utilized, it is clear that there is a large distribution in eccrine sweat glands density specific to regional anatomical surface areas. For example, the volar surfaces of the hand and foot have the highest reported densities approximating greater than 500 glands/cm^2; the skin of dorsal forearm, from which we sampled, has an approximate density of 135–145 glands/cm^2 [25]. If the sweat excreted through the sweat glands to the skin pores can be directed to a collection channel, it can then be analyzed for composition. One of the established techniques is to use a Macroduct sweat collector [26]. The idea is to have a small hole on a plastic piece where sweat is guided through a plastic tube. We have used this idea to create our own design using a moldable plastic polymer called polydimethylsiloxane (PDMS) which is a biocompatible material that is used in microfluidics applications [27,28]. The elastic modulus of PDMS is close to human skin's elastic modulus, which makes PDMS more compatible and comfortable to wear on the skin. Sweat content analysis is traditionally performed by collecting sweat via whole body wash down technique [29] or using absorbent pads [30–34]. It is known that covering the sweat collection area prevents sweat from evaporating resulting in lower local sweat rates and alterations in sweat content, which is known as hydromeiosis, and can be minimized with Macroduct sweat collectors [35]. This method was the basis of our design, where a hole on the PDMS is used to guide the sweat into the sweat collection and analysis channel tubing. Although PDMS is permeable, lab on a chip applications mostly employ PDMS as the building platform as it is practically inert in terms of interactions with biological liquids and constituents [36,37]. Teflon tubing, commonly used in microfluidics devices, was used to guide the sweat as an outlet.

PDMS molds are created by mixing the curing agent with PDMS solution in a 10 to 1 ratio. The solution is mixed for 5 min. The newly formed mixture is then poured into the desired 3D mold (4 cm × 4 cm square with a height of 1 cm) that was printed using a Flashforge 3D printer and ABS as the building material and placed in the vacuum chamber. 3D molds were treated with Methyl ethyl ketone (MEK, or known as butanone) to enhance PDMS curing. PDMS curing agent contains tetramethyl tetravinyl cyclotetrasiloxane that crosslink with PDMS by radical polymerization. However, ABS contains butadiene that has C=C bonds. These bonds react with free radicals in the PDMS crosslinker and significantly reduce even prevent PDMS radical polymerization [38,39]. MEK, on the other hand, contains C=O bonds that do not react with the radicals from crosslinkers. Consequently, MEK coating prevents the cross-linkers from reacting with the butadiene, which allows the curing process to proceed. The vacuum chamber process is done until the PDMS becomes bubble free and transparent. The mold is then placed in the oven to bake at 70 °C for 2–3 h. Once baked and taken out of the oven, the solid PDMS is removed from the 3D mold.

An illustration of the sweat conductivity sensor prototype is given in Fig. 1a. A tube is inserted through a hole that is punched at the center of the PDMS mold. Sweat is collected through the hole and the tube by hydraulic pressure from sweat glands. The PDMS is in contact with the user's skin, and the pressure difference allows the sweat to travel upwards through the tube. Although capillary forces are also present in the tubing, the main force is the sweat secretion from the sweat glands, which acts as a hydraulic pump. Therefore, the increasing pressure in the tube will not have significant effect on sweating mechanisms. Moreover, the tubing is kept short (few centimeters) to just allow sweat draining. Two conductivity sensor wires were placed into the tube using a needle as a thread, from the side of the mold, with one wire above the other (as shown in Fig. 1). Due to the nature of the manual insertion, there will be slight device to device variation in terms of the locations of the wires. However, since each device is characterized and calibrated individually, this variation will not cause issues. The PDMS mold is placed into a wristband with a metal frame that is harvested from a commercial LED watch [40]. The interface circuitry (built on an in-house printed circuit board, PCB) is also placed on top of the PDMS sweat collector. A 22 gauge Teflon tubing is pushed close to the end (but not all the way) to allow sweat go through the punched hole as illustrated in Fig. 1.

The hole to the PDMS was created by a 1.2 mm puncher. The outer and inner diameters of the 22 gauge Teflon tubing were

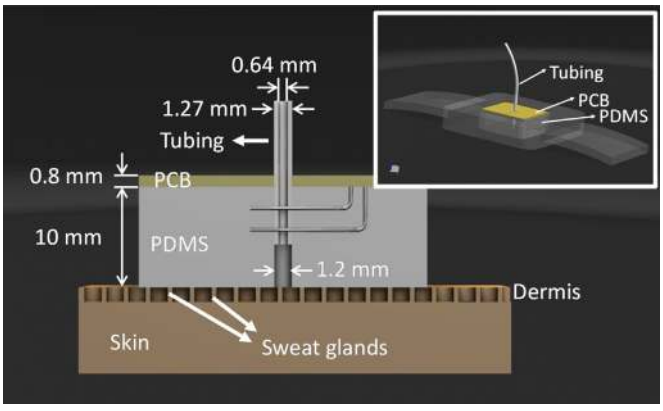

Fig. 1. 3D model of the sweat sensor prototype. Inset shows the overall design including the wrist watch metal frame and wrist band, PDMS sweat collector, and the PCB. PDMS directly touches the skin allowing sweat glands to secrete the sweat through the collection hole and the tubing. As the sweat goes through the tubing, it passes through two wires which are connected to the PCB to measure the conductivity of the sweat.

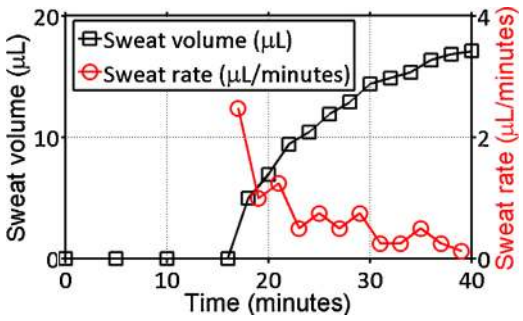

Fig. 2. A representative human sweat collection data using the PDMS sweat collector. Sweat rate decreases as the subject's sweating starts to reach a plateau. A healthy 23 year-old male subject exercised on an exercise bike at his 80% maximum work load. Sweat volume was measured by manually recording sweat levels on the graded tube with markers at every 5 mm.

1.27 mm and 0.64 mm, respectively. The slight difference between the Teflon tubing outer diameter and the PDMS hole (1.2 mm vs. 1.27 mm) makes sure a tight fit exists to prevent any sweat leakage. The tubing was not pushed all the way (kept at 3 mm above the skin) to the skin to avoid any skin irritation from the tube. The thickness of the PDMS was 10 mm. It is important to note here that only the sweat glands that are under the hole will contribute to fill the tube as other sweat glands under the PDMS will be blocked causing hydromeiosis [35]. The approximate number of sweat glands in the area (1.2 mm diameter hole) is 1.5 considering the average sweat gland density of 140 glands/cm^2 for the dorsal forearm [25]. This will ensure at least one sweat gland is present under the hole. Although making the hole size bigger would allow more sweat glands to fill the hole, bigger holes mean more sweat is needed in the tube before it reaches the electrodes. Therefore, we selected the smallest hole size possible to allow us having at least one sweat gland to contribute to the channel.

The wrist watch sweat collector itself was tested for its performance on healthy male ($n = 4$) and female ($n = 1$) subjects. The sweat collector was marked at every 5 mm. Subjects biked at their 80% maximum work load. The time that sweat reached each marker point was recorded and the sweat volume at that moment was calculated using the dimensions of the tubing (0.64 mm inner diameter). The tubing was kept about 35 mm long and the excess sweat was allowed to drip from the end of the tubing. Fig. 2 shows a representative result of a 23 year-old male subject. It takes approximately 15 min for the sweat to appear in the tubing where sweat is visible. This is partly due to the distance of about 1 cm where sweat travels in the PDMS until it reaches to the tubing that is outside the PDMS sweat collector for visual inspection. This initial volume is approximately 5.6 μl which would have taken only few minutes considering the sweat rate is on the order of 2 μl/min. The main delay at this point comes from the initial warming of the body before the sweating starts. The sweat rate was then calculated by taking the derivative of the sweat volume vs. time data set and plotted in Fig. 2.

It is important to note that Fig. 2 does not represent a continuous sweat rate monitoring as this experiment was only used to determine the local sweat rate baseline. Therefore, only a few data points were observed to have an idea on the sweat rate and the viability of the sweat collector itself. As the subject kept the same load of exercise, the sweat rate decreased until a steady state value was reached. This is mainly due to the sweat ducts reaching a steady state secretion level that balances the core temperature of the body with respect to the work load, which is well understood and observed [41–43]. It must further be noted that the sweat rate was only measured on the forearm and therefore cannot be generalized to reflect the whole body sweat rate. It is evident that more sites on the body should be measured to get a better correlation since sweat rate and composition varies throughout the body, which is outside the scope of this current study.

2.2. Impedance analysis of the conductivity sensor

The most common approach for calculating conductivity is to apply an external voltage source to the sample and measure the electric current. In the case of measuring the conductivity of liquid samples, several effects play an important role on the accuracy of the experiment such as double-layer effect, electrode polarization (also known as Faraday's impedance), and the charge-transfer limitation [44,45]. When an electrode emerging into an electrolyte solution, two layers with opposite polarity are formed due to the interaction between the ions and electrodes, which are called inner and outer Helmholtz planes (IHP and OHP). In the IHP (~1 nm), the absorbed ions are attached to the surface of electrode closely [46]. The OHP (~10 nm), on the other hand, acts as a transition region between the electrode and the electrolyte [46]. These two planes form the double-layer capacitance. Also, electrodes are polarized when the solution is excited with an external electric field where ions are diffused onto the electrodes altering the conductivity at the electrode-liquid interface. These effects can be modeled with an equivalent circuit model based on Randle's circuit as shown in Fig. 3b inset [11]. The double-layer effect and electrode polarization can be represented as a double-layer capacitance, C_{dl}, and a Faradic impedance, Z_F. Double-layer capacitance mainly depends on the electrode's material, geometry, and concentration of the electrolyte [45]. It should be noted that since double-layer capacitance is used to model the effect of IHP and OHP, it behaves like a Constant Phase

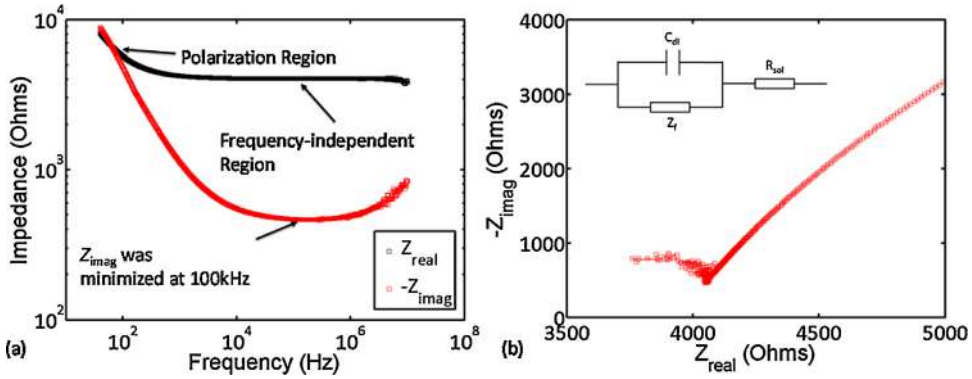

Fig. 3. Bode plot from the EIS for the conductivity sensor with artificial sweat sample. Inset shows the Randel's model circuit. An artificial sweat sample was used on the device at room temperature. (a) Bode plot; (b) Nyquist plot.

Element (CPE) instead of an ideal capacitor, where its impedance value can be expressed as [46]:

$$Z_{\mathrm{CPE}} = \frac{Q}{(j\omega)^n} \tag{1}$$

where Q is the capacitance value, ω is the angular frequency and n is a factor that is smaller than 1. When n is equal to 1, the equation represents an ideal capacitor.

Faradic Impedance, also known as Warburg impedance, can be given as:

$$Z_F = Z_W = \frac{W_{\mathrm{or}}}{\sqrt{\omega}(1-j)\coth(W_{\mathrm{oc}}\sqrt{j\omega})} \tag{2}$$

where W_{or} and W_{oc} are Warburg coefficients for finite length diffusion with a reflective boundary and ω is the angular frequency for the excited signal [45]. As the frequency increases, the Warburg impedance decreases the effect of electrode polarization. Additional components can be added to form a modified Randel's model to include higher order effects such as electrode passivation [11]. These effects were not considered in this study. R_{sol} is defined as the solution resistance.

The excitation signal for the conductivity measurement must be carefully selected to minimize the effects of Randle's circuit components such as unstable reading, corrosion of electrodes, and electrolysis. EIS is primarily used to characterize the frequency response of a conductivity sensor to determine the equivalent circuit model parameters. Since a pair of electrodes was used to detect human perspiration, double-layer capacitance and polarization effects would have an impact on the measurements. Our previous study showed that the double-layer capacitance is around 30 ± 2 pF for Silver wires [11]. An EIS was performed to find the optimum excitation frequency, where these effects were minimized.

The EIS in this study was performed using an Agilent 4294A precision impedance analyzer. The frequency sweep range was between 40 Hz and 10 MHz. The results are shown in Fig. 3. At low frequencies, the solution polarization dominates the measurement resulting a high impedance value. As frequency increases, the effect of electrode polarization becomes negligible since the polarity of the external field switches too fast. When the frequency goes too high (typically in the MHz range), the double-layer capacitance starts shorting the whole circuit causing a high frequency dispersion of the measurement. Physically, the external field switches its polarity before the inner and outer Helmholtz planes are discharged, hence no current flows through the device. In the mid-frequency region, the impedance is practically independent of frequency. From the results of EIS, 100 kHz was chosen as the optimal measurement frequency to eliminate any frequency dependent deviation where both polarization and double-layer capacitance effects are minimal.

2.3. The interfacing circuit

With a goal toward a wearable device, an interfacing circuit was developed and fabricated on a PCB. The circuit consists of an oscillator that provides the excitation signal, sweat conductivity sensor, and a microcontroller with Bluetooth transceiver, as shown in Fig. 4.

An operational amplifier based relaxation oscillator was implemented to provide the 100 kHz AC signal (as chosen from the impedance analysis results) for conductivity measurement. The op-amp configuration works as a relaxation oscillator which has negative and a positive feedback loops, constructed by $(C_1 - R_1)$ and $(R_2 - R_3)$, respectively. When the output of the oscillator is switched, it will change the positive input instantaneously. Yet the voltage on the negative input will change slowly because of the charging/discharging of the series RC circuit on the negative feedback, hence creating a hysteresis. Once the voltage on the capacitor

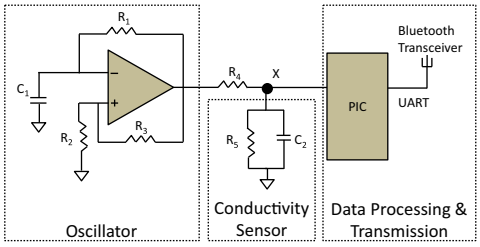

Fig. 4. The circuit diagram of the overall conductivity sensing platform.

reaches its threshold, the output will switch again. Compared to a traditional ring oscillator, relaxation oscillators offer larger tuning ranges and easier implementations [47]. The frequency of the oscillator output (denoted by f) is determined from:

$$f = \frac{1}{2\ \ln 3 R_1 C_1} \tag{3}$$

It should be noted that since the input of the oscillator is controlled by the resistor divider $(R_2 - R_3)$, the relaxation oscillator is susceptible to temperature variations comparing to crystal oscillator-based configurations [48]. Temperature compensation would be needed such as employing opposite temperature coefficient circuit components or dynamic threshold switched-resistor designs in the case of significant environmental temperature changes [49]. We have performed our experiments in room temperature to eliminate the need of temperature compensation.

The conductivity sensor was modeled as a resistor in parallel with a capacitor. R_3 was selected to be 4 kΩ according to the concentration range (detailed in Section 2.4). A 1 kΩ reference resistor R_2 was used in series with the conductivity sensor to form a voltage divider. The effect of C_2 can be neglected at 100 kHz. Therefore, the voltage at node X is directly proportional to the resistance of the sweat which can be related to the resistivity or conductivity.

A PIC16F1823 microcontroller was used to read the voltage values at node X in Fig. 4. The operation clock of the microcontroller is set to 0.5 MHz (2 μs). The signal was sampled by the ADC (Analog to Digital Converter) of the microcontroller every microsecond. Maximum value in every 10 μs (the period of the oscillator circuit) was selected to make sure the logic 1 is properly obtained. The microcontroller is connected to the HC-06 Bluetooth transceiver for wireless transmission of the data reading to a Windows Phone (HTC PM23300). Data processing was done at the monitoring terminal to convert the voltage value into conductivity by using the pre-characterized voltage-conductance and the measured cell-constant. The sweat conductivity sensor and PCB were packaged together to form a wrist-watch type wearable device. Photographs of the device are shown in Fig. 5. The roughness on the PDMS edges is due to the surface tension of PDMS during the curing process in which PDMS rises at the edges in the mold. This roughness does not affect the measurements since the sweat collection occurs on the bottom (flat and smooth) surface of the PDMS. The top of the PDMS is only used for placing the PCB.

2.4. Artificial sweat trials

Sweat composition values vary considerably and should be interpreted in the context of sweat gland activity or whole body sweat rate. However, sweat sodium concentration ranges from 20 to 100 mmol/L; sweat chloride concentration ranges from 26 to 80 mmol/L, and sweat potassium concentration ranges from 2.5 to 6 mmol/L [25,50]. Other compounds or metabolites found in plasma can also be found in discharged sweat in varying concentrations: lactic acid (10 mmol/L), bicarbonate (15–20 mmol/L), urea (15–25 mg/dL), protein (15–25 mg/dL), glucose (0.2–1.2 mg/dL),

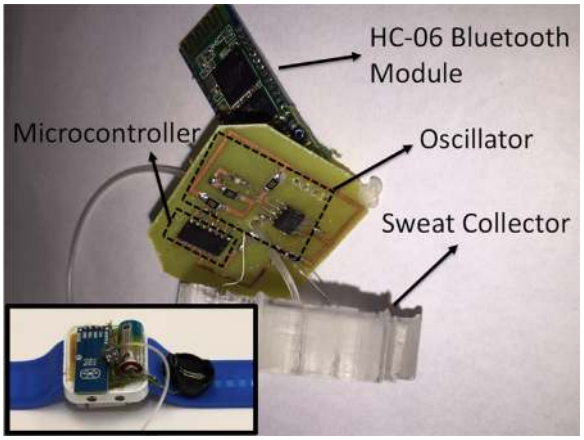

Fig. 5. Photograph of the main parts of the wearable device. Inset shows the overall prototype.

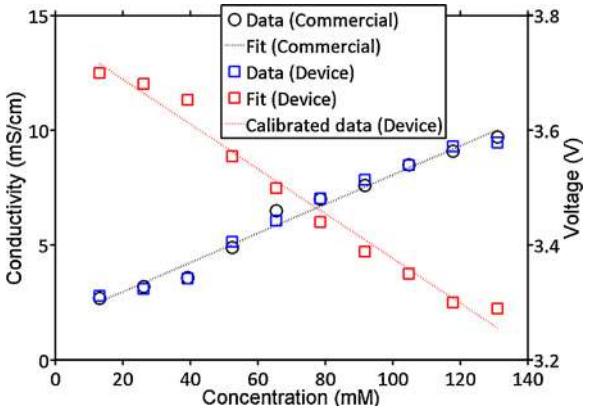

Fig. 6. Device data measured from the output of the microcontroller (in Volts) is calibrated using the commercial sensor data. Linear fit lines, G_{Horiba} (concenration) = a_1 concentration + b_1 and G_{Device} (concenration) = a_2 concentration + b_2 were used for fits with the following values: $a_1 = 0.0636$, $b_1 = 1.7$, $a_2 = -0.0039$, $b_2 = -63.0999$. R^2 and root mean squared error (rmse) values for the commercial sensor data are 0.9817 and 0.367, respectively, and 0.9801 and 0.0234 for the device data, respectively. (For interpretation of the references to color in text near the reference citation, the reader is referred to the web version of this article.)

and ammonia (0.5–8 mmol/L) [50]. In order to determine the viability of a sweat conductivity sensor, artificial sweat can be used so controlled experiments can be conducted rather than relying on real human sweat, which can vary significantly.

According to the European Standard number EN1811: 2012, artificial sweat is concocted by dissolving sodium chloride (NaCl), potassium chloride (KCl), urea, and lactic acid into deionized water (with resistivity of 18.3 MΩ cm). NaCl, KCl, and lactic acid were bought from VWR International, Inc. Urea was supplied from Fisher Scientific, Inc. The weight/volume ratios were 0.5% of NaCl, 0.1% of KCl, 0.1% of lactic acid, and 0.1% of urea. The resulting concentrations were 85 mM for NaCl, 13 mM for KCl, 17 mM for lactic acid, and 16 mM for urea. The standard concentration of artificial sweat is defined as the sum of these four constitutes, which is 131 mM. This total concentration can be considered an average or dehydration situation that would vary from subject to subject [50–53]. Subsequently, other concentrations of artificial sweat were prepared by diluting the standard concentration of artificial sweat. The range for the concentration of artificial sweat was selected to be 13.1–131 mM. The proportion of constitutes was kept at the same ratios but the total concentration was varied. For example, for a diluted artificial sweat that has a total concentration of 13.1 mM electrolytes, its constituents are 8.5 mM for NaCl, 1.3 mM for KCl, 1.7 mM for lactic acid, and 1.6 mM for urea. It should be noted that human sweat contains other compounds besides these four components in artificial sweat, such as calcium, magnesium, minerals, and oils, which could cause slight deviations on the measurements during the real sweat experiments. Since the concentration of those minor compounds is low in human sweat, measuring those four major compounds was found to be sufficient for this study.

Different concentrations of artificial sweat were manually injected into the sweat conductivity sensor to characterize the device. A Horiba LaquaTwin conductivity sensor was used to calibrate the device. The cell constant was calculated to be 40 cm^{-1}. In order to calibrate the microcontroller readings to the commercial sensor readings (Fig. 6), linear fit lines were used as the following (fit parameters are given in Fig. 6 caption). Considering both functions are in the form of $y = ax + b$ with different a and b values (G_{Horiba} (concenration) = a_1 concentration + b_1 and G_{Device} (concenration) = a_2 concentration + b_2), calibrated conductivity was defined as $G_C = AG_{\text{Device}} - B$, where $A = a_1/a_2$ and $B = b_2a_1/a_2 - b_1$. With the current calibration scheme, it can be seen in Fig. 6 that commercial device data (black circles) matches with the calibrated device data (blue squares). Calibration parameters A and B are calculated as −16.3 and −63.1, respectively.

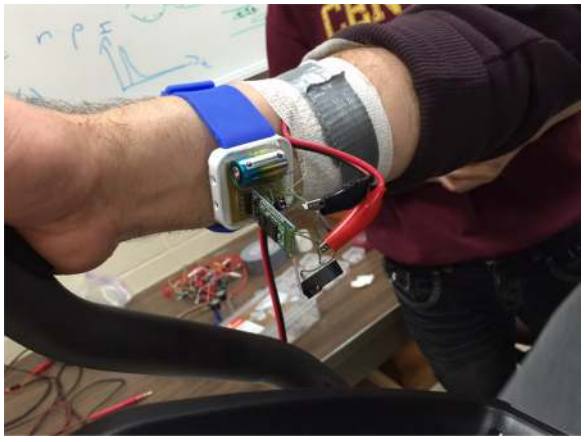

Fig. 7. Subject wearing the proposed device performing exercise.

2.5. Real-time human sweat measurements

Real-time human sweat testing was performed at Central Michigan University. As required by the Institutional Review Board (IRB) at CMU, subject consent was obtained. A total of 4 subjects rode a stationary exercise bike in the laboratory at room temperature while wearing the proposed device. A representative image of one subject is shown in Fig. 7. The maximal aerobic work load was set to 80%, which corresponding to an average heart rate of 144 bpm for this particular test subject shown in Fig. 7.

The efficiency of the sweat collector depends on the sealed contact of the PDMS on the skin. In the case of unsealing, created pressure on the peripheries of the sweat glands area that are not covered by PDMS will be lost causing the collected sweat leak on the opposite side of the sweat flow. This leakage would alter the data acquired afterwards. Therefore, a proper sealing method was investigated. As shown in Fig. 7, PDMS sweat collector was tightly strapped on the forearm. Subjects shaved their arms if needed. Additional probing wires were all stabilized to minimize the movements of the sweat collector. There were few failed attempts on sealed contacts of the sweat collector at the beginning phases of the experiments. However, once optimized, the efficiency of the sweat collection was 100% on 4 subjects.

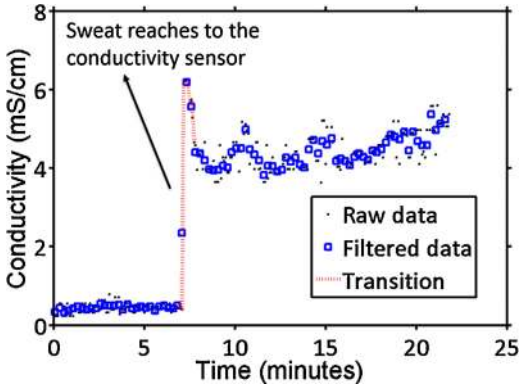

Fig. 8. A representative real-time human subject data. The subject used an exercise bike. The subject was not allowed to intake any liquids during the trial. Raw data were filtered by using a moving average to show the trends. Sweat reached the electrode wires around minute 7 and there was a slight increase in conductivity after 10 min that can be associated with degradation in hydration level.

An HTC PM23300 Windows Phone was used as the monitoring terminal. All received data were recorded and converted into conductivity values. Results are plotted in Fig. 8. Raw data was filtered by performing data averaging where every 3 data points were averaged. There was an average latency of 7 min for sweat to reach the sensing area. It must be noted that this latency is much lower than the sweat rate tests (15 min) because the sensing wires were inserted within the collection channel allowing the device sense the conductivity earlier. Since the subject was not allowed to intake any fluids during the experiment, a slight conductivity increase was observed (transition data points are labeled in Fig. 8) and the measured conductivity values range from 3.6 mS/cm to 5.6 mS/cm, which is consistent with previous sweat conductivity measurements [1,11]. The initial high conductivity and sudden decay reading at the beginning of the first minutes of readings was consistent with other experiments [11,54,55]. This phenomenon can be attributed to the sample contamination resulting from the salts and minerals on the skin prior to exercise. Previously, an elevated mineral content was found in the collected sweat in the first hours of exercise, which is consistent to what had previously been reported [54]. However when the skin was cleaned prior to exercise, this mineral content was lower, suggesting that the initial abnormal high conductivity value is likely due to minerals found on the skin before the exercise. We made sure to clean the skin with DI water prior to exercise and let the skin air dry to minimize the previous skin content. As the exercise continues, an increase in conductivity was observed (after 10 min), hinting increasing sweat conductivity concentration. Although sweat conductivity does not change unless exceeding maximum capability of sweat glands to harvest ions from sweat, this slight increase in conductivity may be correlated to subject's hydration state during the exercise due to the combined sweating and lack of proper fluid intake. Sweat composition changes during dehydration process as the body conserves water to ensure central blood volume is maintained so blood pressure does not fall. This would tend to increase the concentration of sweat electrolyte as the amount of water "donated" by the body to sweating decreases and is reallocated to ensure plasma volume is maintained [56]. As the concentration changes, the conductivity of sweat electrolyte would therefore change. Moreover, as the sweat rate increases, electrolyte reabsorption in the sweat gland ducts decreases leading to increased electrolyte loss with sweating [38,60,61]. Excessive exercise or activity causes sweat becoming more "salty" resulting an increase in the conductivity of sweat [11,62]. The measured sweat conductivity (around 4 mS/cm) corresponds to a sodium concentration of 23 mM, which is consistent with the results observed from sodium ISE [1]. It proves that the proposed sweat sensing system could monitor the conductivity level of one's perspiration without any other external instrument.

During the exercise, the different skin temperature would affect the temperature of sweat electrolyte, which eventually alter the conductivity measurement. It was shown in [11] that the temperature change affects the measured conductivity in artificial sweat. The temperature would affect the activity coefficient of sweat electrolyte based on Debye-Huckel limiting law and the disassociation of weak electrolyte. Therefore, on a separate experiment, we have monitored the temperature inside the tube using a K-type thermocouple. The sensing tip of the thermocouple was punched inside the PDMS channel. A microcontroller was connected with the thermocouple to read and display the temperature data. We found out that as the subject starts exercising, a thermal equilibrium was quickly established at room temperature. The temperature inside the tube was found to be stable at 28 °C during the entire measurement as it rose from 23 °C. Building upon the fact that a thermal equilibrium quickly established in our experiments, we conclude that the temperature should not be an issue for the conductivity measurement in this study. However, if the environmental temperature varies significantly, the thermal equilibrium would change dramatically thus resulting in temperature drifting of the conductivity measurement. In this case, a temperature sensor, like the thermocouple, will be necessary for the system to provide the real-time information for the microcontroller. The microcontroller can compensate the temperature drifting based on the pre-determined conductivity-temperature function.

3. Conclusions

In this paper, we reported the design, fabrication and testing of a wearable sweat conductivity sensing device. The system was proven to achieve wireless non-invasive monitoring of human sweat conductivity without the usage of external instruments. A PDMS-based sweat collector was proposed and its functionality was demonstrated. EIS study reveals the electrochemical dynamics of the conductivity measurement for sweat electrolytes. The interface circuit was designed and implemented to facilitate the electrochemical dynamics of the sweat conductivity sensor. The sweat collector, conductivity sensor, and the interfacing circuit on PCB were packaged together to form a wearable device.

The minimum required volume to obtain measurements depends on the size of the collection channels or tubes. It is reasonable to compare different sweat sensors for the minimum time to get their first reading. It took around 10 min in [1] and 17 min in [2]. In our study, it took around 7–20 min to get the first reading. The concentrations of sweat compounds as well as the rate of sweat are highly individual and vary significantly depending on gender, fitness level, diet, environment, and the exercise or work load involved [25,33,37,57–59]. Therefore, a direct comparison on cross studies does not give conclusive results.

The artificial and human sweat experiments demonstrated very promising results for the device, which, potentially, provides a great contribution to the wearable device research area regarding to sweat sensing. This proof-of-concept for a device allowed us to measure sweat conductivity and hopefully will lead to estimates of sweat osmolality. With further validation of the device and the addition of a sweat rate sensor, we may then investigate the relationship between conductivity and hypo or hyperhydration. Also, in order to get an estimation of a full body dehydration, body mass loss measurement sensors could be combined with current conductivity sensor. For a sweat-based hydration device, it must be calibrated individually as the sweat profile would change person-to-person.

Acknowledgements

The authors would like to thank Dr. Axel Mellinger for allowing us use his Impedance Analyzer and helping us obtaining good quality photo images.

References

[1] A.J. Bandodkar, D. Molinnus, O. Mirza, T. Guinovart, J. Windmiller, G. Valdes-Ramirez, F.J. Andrade, M.J. Schoning, J. Wang, Epidermal tattoo potentiometric sodium sensors with wireless signal transduction for continuous non-invasive sweat monitoring, Biosens. Bioelectron. 54 (April) (2014) 603–609.
[2] B. Schazmann, D. Morris, C. Slater, S. Beirne, C. Fay, R. Reuveni, D. Diamond, A wearable electrochemical sensor for the real-time measurement of sweat sodium concentration, Anal. Methods 2 (January (4)) (2010) 342–348.
[3] R.J. Maughan, S.M. Shirreffs, Development of hydration strategies to optimize performance for athletes in high-intensity sports and in sports with repeated intense efforts, Scand. J. Med. Sci. Sports 20 (May) (2010) 59–69.
[4] M.N. Sawka, L.M. Burke, R. Eichner, R.J. Maughan, S.J. Montain, N.S. Stachenfeld, Exercise and fluid replacement: position stand, J. Am. Coll. Sports Med. 39 (2) (2007) 377–390.
[5] R. Carter, S.N. Cheuvronta, D.W. Wrayb, M.A. Kolkaa, L.A. Stephensona, M.N. Sawkaa, The influence of hydration status on heart rate variability after exercise heat stress, J. Therm. Biol. 30 (October (7)) (2005) 495–502.
[6] S.N. Cheuvront, M.N. Sawkaa, Hydration assessment of athletes, Sports Sci. Exch. 97 18 (2) (2015).
[7] D. Morris, S. Coyle, Y. Wu, K. Lau, G. Wallace, D. Diamond, Bio-sensing textile based patch with integrated optical detection system for sweat monitoring, Sens. Actuators B. 139 (May (1)) (2009) 231–236.
[8] M. Alomari, G. Liu, A. Mueller, A. Mock, R.N. Ghosh, K. Smith, T. Kaya, A portable optical human sweat sensor, J. Appl. Phys. 116 (November (18)) (2014).
[9] A.J. Bandodkar, W. Jia, J. Wang, Tattoo-based wearable electrochemical devices: a review, Electroanalysis 27 (March (3)) (2015) 562–572.
[10] G. Liu, K. Smith, T. Kaya, Implementation of a microfluidic conductivity sensor – a potential sweat electrolyte sensing system for dehydration detection, in: 36th Annual International Conference of the IEEE Engineering in Medicine and Biology Society, Chicago, IL, USA, August 26–30, 2014, pp. 1678–1681.
[11] G. Liu, M. Alomari, B. Sahin, S.E. Snelgrove, J. Edwards, A. Mellinger, T. Kaya, Real-time sweat analysis via alternating current conductivity of artificial and human sweat, Appl. Phys. Lett. 106 (March 13) (2015).
[12] Z. Chang, G.A.M. Pop, G.C.M. Meijer, A comparison of two- and four-electrode techniques to characterize blood impedance for the frequency range of 100 Hz to 100 MHz, IEEE Trans. Biomed. Eng. 55 (March (3)) (2008) 1247–1249.
[13] J. Yu, C. Liu, Microfabricated thin film impedance sensor & AC impedance measurements, Sensors 10 (June (6)) (2010) 5845–5858.
[14] J. Park, S. Kim, I. Park, A multi-pair electrode based impedance sensing biopsy needle for tissue discrimination during biopsy process, in: 36th Annual International Conference of the IEEE Engineering in Medicine and Biology Society, Chicago, IL, USA, August 26–30, 2014, pp. 1695–1698.
[15] X. Huang, R.W. Pascal, C.J. Banks, M. Mowlem, H. Morgan, A miniature, high precision conductivity and temperature sensor system for ocean monitoring, IEEE Sens. J. 11 (December (12)) (2011) 3246–3252.
[16] Fitbit Inc., Specifications of Fitbit Charge. Available at: https://www.fitbit.com/charge#specs (online).
[17] LG Electronics, Technical Specifications of G-Watch. Available at: http://www.lg.com/us/smartwatch/g-watch-r (online).
[18] Polar Electro, Features of Polar RS300X. Available at: http://www.polar.com/us-en/products/improve_fitness/running_multisport/RS300X (online).
[19] S.C. Mukhopadhyay, Wearable sensors for human activity monitoring: a review, IEEE Sens. 15 (March (3)) (2015) 1321–1330.
[20] Z. Popovic, P. Momenroodaki, R. Scheeler, Toward wearable wireless thermometers for internal body temperature measurements, IEEE Commun. Mag. 52 (October (10)) (2014) 118–125.
[21] J. Gomez-Clapers, R. Casanella, A fast and easy-to-use ECG acquisition and heart rate monitoring system using a wireless steering wheel, IEEE Sens. 12 (March (3)) (2012) 610–616.
[22] M. Oner, J.A. Pulcifer-Stump, P. Seeling, T. Kaya, Towards the run and walk activity classification through step detection – an android application, in: 34th Annual International Conference of the IEEE Engineering in Medicine and Biology Society, San Diego, CA, USA, August, 2012, pp. 1980–1983.
[23] P. Salvo, F.D. Francesco, D. Costanzo, C. Ferrari, M.G. Trivella, D. De Rossi, A wearable sensor for measuring sweat rate, IEEE Sens. 10 (October (10)) (2010) 1557–1558.
[24] E.R. Nadel, R.W. Bullard, J.A.J. Stolwijk, Importance of skin temperature in the regulation of sweating, J. Appl. Physiol. 31 (July (1)) (1971) 80–87.
[25] N.A. Taylor, C.A. Machado-Moreira, Regional variations in transepidermal water loss, eccrine sweat gland density, sweat secretion rates and electrolyte composition in resting and exercising humans, Extreme Physiol. Med. 2 (February (4)) (2013).
[26] Macroduct® Sweat Collection System. Available at: http://www.elitechgroup.com/corporate/products/market-segment/clinical-chemistry/cystic-fibrosis-sweat-tests/macroduct-r-sweat-collection-system-ref13/overview (online).
[27] N. Triroj, M.A. Lapierre-Devlin, S.O. Kelley, R. Beresford, Microfluidic three-electrode cell array for low-current electrochemical detection, IEEE Sens. 6 (December (6)) (2006) 1395–1402.
[28] D.A. Chang-Yen, D.G. Myszka, B.K. Gale, A novel PDMS microfluidic spotter for fabrication of protein chips and microarrays, J. Microelectromech. Syst. 15 (October (5)) (2006) 1145–1151.
[29] S. Shrreffs, R. Maughan, Whole body sweat collection in humans: an improved method with preliminary data on electrolyte content, J. Appl. Physiol. 82 (1) (1997) 336–341.
[30] H. Ueda, Y. Inoue, Improved procedure for estimating time-dependent changes in local sweat rates by measuring local sweat volumes, J. Ergon. (2013).
[31] G. Havenith, A. Fogarty, R. Bartlett, C.J. Smith, V. Ventenat, Male and female upper body sweat distribution during running measured with technical absorbents, Eur. J. Appl. Physiol. 104 (2) (2008) 245–255.
[32] M.J. Patterson, S.D. Galloway, M.A. Nimmo, Variations in regional sweat composition in normal human males, Exp. Physiol. 85 (6) (2000) 869–875.
[33] L.B. Baker, J.R. Stofan, A.A. Hamilton, C.A. Horswill, Comparison of regional patch collection vs. whole body washdown for measuring sweat sodium and potassium loss during exercise, J. Appl. Physiol. 107 (3) (2009) 887–895.
[34] L.B. Baker, C.T. Ungaro, K.A. Barnes, R.P. Nuccio, A.J. Reimel, J.R. Stofan, Validity and reliability of a field technique for sweat Na+ and K+ analysis during exercise in a hot-humid environment, Physiol. Rep. 2 (5) (2007).
[35] M.R. Ely, B.R. Ely, T.D. Chinevere, C.P. Lacher, H.C. Lukaski, S.N. Cheuvront, Evaluation of the Megaduct sweat collector for mineral analysis, Physiol. Meas. 33 (3) (2012) 385.
[36] S. Haeberle, R. Zengerle, Microfluidic platforms for lab-on-a-chip applications, Lab Chip 7 (9) (2007) 1094–1110.
[37] P. Dittrich, A. Manz, Lab-on-a-chip: microfluidics in drug discovery, Nat. Rev. Drug Discov. 5 (3) (2006) 210–218.
[38] L.Y. Tyng, M.R. Ramli, M.B.H. Othman, R. Ramli, Z.A.M. Ishak, Z. Ahmad, Effect of crosslink density on the refractive index of a polysiloxane network based on 2,4,6,8-tetramethyl-2,4,6,8-tetravinylcyclotetrasiloxane, Polym. Int. 62 (3) (2013) 382–389.
[39] J.E. McMurry, Organic Chemistry, 7th ed., 2008, pp. 1207–1208.
[40] Unisex Royal Blue LED Mirror Digital Sports Watch. Available at: http://www.amazon.com/Unisex-Mirror-Digital-Sports-Silicone/dp/B00K34Z0W6 (online).
[41] R.W. Bullard, Continuous recording of sweating rate by resistance hygrometry, J. Appl. Physiol. 17 (4) (1962) 735–737.
[42] C.A. Machado-Moreira, F.M. Smith, A.M. van den Heuvel, I.B. Mekjavic, N.A. Taylor, Sweat secretion from the torso during passively-induced and exercise-related hyperthermia, Eur. J. Appl. Physiol. 104 (2) (2008) 265–270.
[43] Y.J. Fan, Determination of Heat Acclimatization by Capacitance Hygrometer-Sweat Capture Capsule Method, 1987.
[44] P. Mirtaheri, S. Grimnes, Ø.G. Martinsen, Electrode polarization impedance in weak NaCl aqueous solutions, IEEE Trans. Biomed. Eng. 52 (December (12)) (2005) 2093–2099.
[45] F. Scholz, The Electrical Double Layer and its Structure, in: Electroanalytical Methods Guide to Experiments and Applications, 2nd ed., Springer, Berlin, 2010.
[46] E. Barsoukov, J.R. Macdonald, The Electrical Analogs of Physical and Chemical Processes, in: Impedance Spectroscopy: Theory, Experiment, and Applications, 2nd ed., John Wiley & Sons, New York, 2005.
[47] Y. Tokunaga, S. Sakiyama, A. Matsumoto, S. Dosho, An on-chip CMOS relaxation oscillator with voltage averaging feedback, IEEE J. Solid-State Circuits 45 (June (6)) (2010) 1150–1158.
[48] U. Denier, Analysis and design of an ultralow-power CMOS relaxation oscillator, IEEE Trans. Circuits Syst. I: Regul. Pap. 57 (August (8)) (2010) 1973–1982.
[49] Q. Yu, Z. Xu, N. Ning, Y. Guan, B. Chen, Design of a relaxation oscillator with low power-sensitivity and high temperature-stability, Electr. Eng. Control 98 (2011) 421–429.
[50] K. Sato, W. Kang, K. Sage, K. Sato, Biology of sweat glands and their disorders: I. Normal sweat gland function, J. Am. Acad. Dermatol. 20 (April (4)) (1989) 537–563.
[51] S.F. Godek, C. Peduzzi, R. Burkholder, S. Condon, G. Dorshimer, A.R. Bartolozzi, Sweat rates, sweat sodium concentrations, and sodium losses in 3 groups of professional football players, J. Athl. Train. 45 (4) (2010) 364.
[52] M.J. Buono, K.D. Ball, F.W. Kolkhorst, Sodium ion concentration vs. sweat rate relationship in humans, J. Appl. Physiol. 103 (3) (2007) 990–994.
[53] A.R. Bartolozzi, S.F. Godek, C. Peduzzi, J. Kopec, R. Burkholder, Sweat sodium concentration in NFL players during dietary sodium Supplementation compared to when they are not supplemented, Med. Sci. Sports Exerc. 40 (Suppl.) (2008) S86.
[54] M.R. Ely, R. Kenefick, S.N. Cheuvront, T.D. Lacher, H.C. Lukaski, S.J. Montain, Surface contamination artificially elevates initial sweat mineral concentrations, J. Appl. Physiol. 110 (2011) 1534–1540.
[55] S. Coyle, K.-T. Lau, N. Moyna, D. O'Gorman, D. Diamond, F. Di Francesco, D. Costanzo, P. Salvo, M.G. Trivella, D.E. De Rossi, N. Taccini, R. Paradiso, J.-A. Porchet, A. Ridolfi, J. Luprano, C. Chuzel, T. Lanier, F. Revol-Cavalier, S. Schoumacker, V. Mourier, I. Chartier, R. Convert, H. De-Moncuit, C. Bini, BIOTEX – biosensing textiles for personalised healthcare management, IEEE Trans. Inf. Technol. Biomed. 14 (2) (2010) 364–370.
[56] R.M. Morgan, M.J. Patterson, M.A. Nimmo, Acute effects of dehydration on sweat composition in men during prolonged exercise in the heat, Acta Physiol. Scand. 182 (1) (2004) 37–43.

[57] F.T. Amorim, A.C. Vimieiro-Gomes, C.A. Machado-Moreira, F.C. Magalhaes, M.S. Rose, L.S. Prado, L.O.C. Rodrigues, Is sweat rate during steady state exercise related to maximum oxygen uptake? J. Therm. Biol. 31 (6) (2006) 521–525.
[58] N.B. Morris, M.N. Cramer, S.G. Hodder, G. Havenith, O. Jay, A comparison between the technical absorbent and ventilated capsule methods for measuring local sweat rate, J. Appl. Physiol. 114 (6) (2013) 816–823.
[59] D. Gagnon, G.P. Kenny, Sex differences in thermoeffector responses during exercise at fixed requirements for heat loss, J. Appl. Physiol. 113 (5) (2012) 746–757.
[60] H. Tanaka, Y. Osaka, S. Obara, H. Yamaguchi, H. Miyamoto, Changes in the concentrations of Na+, K+, and Cl− in secretion from the skin during progressive increase in exercise intensity, Eur. J. Appl. Physiol. 64 (6) (1992) 557–561.
[61] M.J. Buono, R. Claros, T. DeBoer, J. Wong, Na+ secretion rate increases proportionally more than Na+ reabsorption rate with increases in sweat rate, J. Appl. Physiol. 105 (4) (2008) 1044–1048.
[62] A.K. Shamsuddin, T. Kuwahara, A. Oue, C. Nomura, S. Koga, Y. Inoue, N. Kondo, Effect of skin temperature on the ion reabsorption capacity and sweat glands during exercise in humans, Eur. J. Appl. Physiol. 94 (4) (2005) 442–447.

Biographies

Gengchen Liu was born in Beijing, China, in 1993. He received the B.S. and B.Eng. degrees in electrical engineering and communication engineering from Central Michigan University, Mount Pleasant, and North China University of Technology, Beijing, both in 2015. From 2013 to 2015, he was an undergraduate researcher in Dr. Tolga Kaya's sensor group at Central Michigan University. His research interests include microelectronics circuit design, and biomedical sensors. Mr. Liu received the Central Michigan University president's award for undergraduate research and creative accomplishments. He is an IEEE Student member.

Che Ting Ho is currently working toward her B.S. degree in mechanical engineering at Central Michigan University, Mount Pleasant. Starting from 2013, she has been on Dr. Tolga Kaya's research team. She focuses on the design and fabrication of devices for various research projects. Her research interests include biosensors and materials science. She is also interested in product design. Ms. Ho has been awarded Dean's list honors for her academic performance at Central Michigan University. She also received CMU's Undergraduate Research and Creative Endeavors Grant and 2015–2016 Stephenson Engineering Scholarship. She was also a candidate for National Barry Goldwater Scholarship. Ms. Ho is the vice president of the Society of Women Engineers at CMU.

Nathaniel Slappey III was born in Detroit, Michigan, in 1992. He received the B.S. degree in mechanical engineering from Central Michigan University, Mount Pleasant, in 2015. From 2013 to 2015, he was an undergraduate student researcher. His research interests include hydration analysis, PDMS microfluidic design for biomedical purpose.

Zhixuan Zhou received the B.S. degree in electrical engineering with a minor in mathematics from Central Michigan University, Mount Pleasant, in 2015. He was in Dr. Kaya's research group since 2014. His research interests include circuit design and printed circuit board fabrication.

Samuel E. Snelgrove is originally from Winchester, Virginia. He received his B.S. degree in athletic training from James Madison University in 2013, and M.A. degree in exercise physiology at Central Michigan University, Mount Pleasant, in 2015. From 2014 he started work with Dr. Kaya's research group. His research interest includes sweat analysis and dehydration study.

Marc Brown was born in Oceanside, California in 1991. He received B.S. degree from Central Michigan University, Mount Pleasant, in 2015. From 2011 to 2014, he was a Co-Op for The Dow Chemical Company. His work at Dow involved a wide range of topics from spectroscopy to digital signal processing. Mr. Brown is a student member of IEEE. He graduated with *Cum Laude*.

Alexander Grabinski was born in Novi, Michigan, in 1992. He received B.S. degree in mechanical engineering from Central Michigan University, Mount Pleasant, in 2015. In 2014 he worked from Ford Motor Company at the Livonia Transmission Plant. His duties primarily with the 6R1 and 6R3 transmission lines. He will be working full time at Ford in product development as a part of the Ford College Graduate program come June. Mr. Grabinski has been awarded Dean's list honors for his academic performance at Central Michigan University.

Xiaoju Guo was born in Shenyang, China, in 1993. She received B.S. degree in electrical engineering from Central Michigan University, Mount Pleasant, and B.Eng. degree in communication engineering from North China University of Technology, Beijing, both in 2015. From 2013 to 2015, she was an undergraduate researcher in Dr. Kaya's research group. Her research interests include microcontroller programming and android application developments. Ms. Guo has been awarded Dean's list honors for her academic performance at Central Michigan University several times.

Yuhao Chen received his B.S. degree in mechanical engineering from Central Michigan University, Mount Pleasant, in 2015. He was in Dr. Kaya's senior design team since 2014. He focused on CAD design and drawing.

Kevin Miller received B.S. degree from University of Wisconsin-Green Bay, M.S. degree from University of Wisconsin-LaCrosse, and his Ph.D. from Brigham Young University. He holds an Associate Professor position in the department of rehabilitation and medical sciences at Central Michigan University, Mount Pleasant. His research interests include study of the treatment, prevention and causes of exercise-associated muscle cramping hydration. Dr. Miller is a member of National Athletic Trainers' Association.

Jeffrey E. Edwards received his M.S. degree in exercise physiology from Ball State University and his Ph.D. in human performance with emphasis in the areas of physiology and human performance from Indiana University. His research work has addressed the measurement of energy expenditure of physical activities using respiratory calorimetry as well as stable isotopic methods of measuring energy metabolism. For the last several years, he focused on the neuromuscular area and investigations have ranged from arthrogenic muscle inhibition to measurement of neuromuscular excitability changes during training. Dr. Edwards used to be a member of the Board of Trustees of the Midwest American College of Sports Medicine, as well as its past president.

Tolga Kaya received his B.S., M.S., and Ph.D. degrees in electronics engineering from Istanbul Technical University, Istanbul, Turkey. He currently holds a joint Associate Professor position in the School of Engineering and Technology and the Science of Advanced Materials program at Central Michigan University, Mount Pleasant. His research interests are analog VLSI circuit design, MEMS sensors and energy harvesting systems. His research is also involved in biomedical engineering where bacterial hydrodynamics are studied under various shear flow regimes to enlighten the bacterial infections in catheterized patents.